# Development of Gd-Enriched Alloys for Spent Nuclear Fuel Applications—Part 1: Preliminary Characterization of Small Scale Gd-Enriched Stainless Steels

*C.V. Robino, J.N. DuPont, R.E. Mizia, J.R. Michael, D.B. Williams, and E. Shaber*

*(Submitted 15 November 2002)*

**The influence of Gd additions on the microstructure and hardness of type 316L stainless steel was investigated by various microstructural characterization techniques. This work was conducted as a first step toward the development of Gd-enriched alloys for spent nuclear fuel applications. Small (~10 g) gas tungsten arc melt buttons were prepared to produce 316L stainless steel with Gd levels from 0.1-10 wt.% Gd. Electron microprobe measurements showed that Gd is essentially insoluble in the austenite/ferrite matrix. All of the alloys formed an interdendritic (Fe, Ni, Cr)$_3$Gd intermetallic, and the amount of the (Fe, Ni, Cr)$_3$Gd phase increased with increasing Gd concentration. Depending on the P and O levels, various amounts of Gd phosphides and oxides were also observed. The relatively high Ni concentration (~28 wt.% Ni) and low Cr concentration (~3 wt.% Cr) of the (Fe, Ni, Cr)$_3$Gd phase led to Ni depletion and Cr enrichment in the matrix which, in turn, affected the matrix stability. Alloys with 0.1-6 wt.% Gd exhibited a two-phase ferrite/austenite matrix. Alloys containing 8 and 10 wt.% Gd exhibited a fully ferritic matrix due to extensive Ni depletion/Cr enrichment and concomitant stabilization of ferrite. Hardness increased with increasing Gd concentration due to the formation of the (Fe, Ni, Cr)$_3$Gd intermetallic and the change in matrix structure from austenite to ferrite. A mass balance procedure is presented that accounts for changes to the matrix composition with Gd concentration. This procedure can be used to determine the nominal alloy composition required to produce a 316L-type matrix composition for any Gd level.**

**Keywords** gadolinium, neutron absorbing material, nuclear criticality safety, solidification, stainless steel

## 1. Introduction

Safe disposition of spent nuclear fuel requires the identification and development of materials for criticality control. These materials may be used for the internal baskets that support spent fuel assemblies and serve the following three functions: (1) structural support, (2) spent nuclear fuel geometry control, and (3) nuclear criticality safety. In addition, the basket materials must be corrosion resistant under the projected storage conditions. Recent research on selection of candidate basket alloys, which could meet these requirements, has considered stainless steels containing boron.[1,2] While these alloys are available as ASME code-approved materials, gadolinium (Gd) may be more effective than boron (B) as an alloy addition for neutron absorption for two reasons. First, Gd has a significantly higher neutron absorption cross section than B.[3] Second, Gd-containing constituents in the alloy may not dissolve as quickly as chromium borides in the presence of water during basket material degradation due to long term corrosion.[3] Therefore, there is now interest in the use of Gd-containing alloys for storage, transport, and disposal of spent nuclear fuel. However, unlike stainless steel alloys containing B, there has been very little research on the fabrication, microstructure, and resultant mechanical and physical properties of Gd-containing alloys. To meet the functional requirements of a neutron absorber material, Gd should be alloyed into a corrosion resistant metallic matrix of stainless steel or Ni-base alloy.[4] Given the large quantities of material required, it is desired that the material be producible by conventional fabrication methods such as ingot casting and hot working. Ultimately, the material will be formed and welded into an internal structure that will cradle the fuel and maintain a specified geometry.[4]

In view of these requirements, a detailed understanding of the composition-processing-microstructure-property relationships of Gd-enriched stainless steels and Ni-base alloys is required for successful alloy development. However, there are very few data concerning the basic physical metallurgy of Gd-enriched alloys in the open literature. The only information concerning the relevant ternary systems consists of a partial isothermal section (at 25 °C) for the Fe-Ni-Gd system.[5] Phase diagrams for the relevant binary systems, e.g., Fe-Gd, Ni-Gd, and Cr-Gd, are available.[6,7] The binary Fe-Gd and Ni-Gd systems both contain numerous intermetallic phases and undergo complex solidification sequences. In particular, peritectic reactions appear to dominate the formation of intermetallic compounds in these systems (with the notable exception of low Gd levels in the Ni-Gd system, where a eutectic reaction is observed). Moreover, no information regarding solidification path information (i.e., the constituents that form during solidification as a function of melt composition) could be found for any of the relevant systems.

**C.V. Robino** and **J.R. Michael,** Sandia National Laboratories, Albuquerque, NM; **J.N. DuPont** and **D.B. Williams,** Department of Materials Science and Engineering, Lehigh University, Bethlehem, PA; and **R.E. Mizia** and **E. Shaber,** Idaho National Engineering and Environmental Laboratory, Idaho Falls, ID. Contact e-mail: cvrobin@sandia.gov.

**Table 1 Composition of Base 316L Alloy Determined by ICP-MS**

| Element | Concentration, wt.% |
|---|---|
| C | 0.017 |
| Mn | 1.75 |
| P | 0.031 |
| S | 0.002 |
| Si | 0.45 |
| Cr | 16.33 |
| Ni | 10.94 |
| Mo | 2.89 |
| Cu | 0.32 |
| N | 0.04 |
| Fe | Balance |

As a first step toward developing canister materials for transportation and storage of highly enriched spent nuclear fuel, the primary objective of the current research is to gain a basic understanding of the composition-microstructure-processing relations of stainless steels and Ni-base alloys enriched with Gd. The results of this research will be presented in three separate articles. Part 1, presented here, provides preliminary results from analyses conducted on small scale heats of 316L stainless steel enriched with varying levels of Gd, from 0.1-10 wt.% Gd. The main objective of Part 1 is to understand the influence of Gd concentration on the type, amount, and composition of phases that form. This information has been used to produce large scale heats of Gd enriched 316L stainless steel over a narrower Gd range (0.1-6 wt.% Gd), which were subjected to more detailed analysis by microstructural characterization, differential thermal analysis, heat treatment studies, and hot ductility testing (to be presented in Part 2). Lastly, preliminary results from a Gd enriched Ni-base alloy will be presented in Part 3.

## 2. Experimental Procedure

Gas-tungsten arc (GTA) melt buttons (approximately 10 g mass) were fabricated by arc melting in an inert environment. The buttons were made by mixing 316L stainless steel (composition reported in Table 1) and high purity Gd (99.9%). Various proportions of the 316L and Gd were weighed to a tenth of a mg. After pumping down to less than 2.7 Pa (20 millitorr), the GTA melting chamber was backfilled with ultra high purity argon, and this cycle was repeated three times. The buttons were melted and flipped 3-4 times to ensure homogeneity. Ten GTA melt buttons were prepared with the following Gd concentrations: 0.1, 0.2, 0.4, 1, 1.5, 2, 4, 6, 8, and 10 wt.% Gd. Hardness measurements were made on the melt buttons using a Rockwell indenter with the A scale.

Light optical microscopy (LOM) was conducted on unetched samples polished through 0.04 μm colloidal silica. Scanning electron microscopy (SEM) was performed using a JEOL (JEOL USA, Peabody, MA) 6300 field emission gun scanning electron microscope (FEG-SEM) at an accelerating voltage of 15 kV. Quantitative image analysis (QIA) was performed to determine the total volume fraction of secondary phases. Area fractions of secondary phases were measured using both LOM and SEM. The SEM photomicrographs were acquired in the back-scattered electron mode. Area fractions were assumed to be equivalent to volume fractions. Electron probe microanalysis (EPMA) was conducted on a JEOL 733 equipped with wavelength dispersive spectrometers, and operated at an accelerating voltage of 15 kV and beam current of 20 nA. The EPMA samples were mounted in epoxy resin, polished flat to a 0.3 μm finish using an alumina slurry, ultrasonically cleaned in acetone, and carbon coated prior to analysis. Raw data were reduced to weight percentages (wt.%) using an atomic number, absorption, fluorescence (ZAF) algorithm.[8]

**Table 2 Comparison of Atomic Radii and Room Temperature Crystal Structures of Gd, Fe, Ni, and Cr**

| Element | Atomic Radius, nm | Room Temperature Crystal Structure |
|---|---|---|
| Gadolinium | 0.161 | Hexagonal |
| Iron | 0.124 | Body Centered Cubic |
| Nickel | 0.125 | Face Centered Cubic |
| Chromium | 0.125 | Body Centered Cubic |

Electron backscattered diffraction (EBSD) patterns were collected using a JEOL 6400 SEM using a charge coupled device (CCD)-based camera system. Patterns were obtained from samples using 20 kV accelerating voltage, 10 nA beam current, and 70° specimen tilt. The patterns were collected by stopping the electron beam on the feature or area of interest. The CCD camera acquisition time was controlled by automatic blanking of the electron beam. Typical exposure times for this study were in the range of 2-10 s. The raw patterns were corrected for the background intensity using a flat-fielding procedure. Qualitative chemistry information was obtained through x-ray energy dispersive spectrometry (EDS), and the crystallographic information was automatically extracted from the patterns using software developed at Sandia National Laboratories (Albuquerque, NM). The crystallographic information along with the qualitative chemistry information was used to search the International Center for Diffraction Data (ICDD) Powder Diffraction File (PDF) for candidate matches.

## 3. Results

Considering the relevant binary phase diagrams and the large mismatch in atomic radius and room temperature crystal structure between Gd and the main alloying elements of stainless steel (i.e., Fe, Ni, Cr), Table 2, it was expected that the matrix of stainless steel would not dissolve significant amounts of Gd. In this case, the majority of Gd would exist as one or more secondary phases. LOM images of typical microstructures are shown in Fig. 1 for the 0.2, 2.0, 4.0, and 6.0 wt.% Gd melt buttons. Alloys with 0.1-6 wt.% Gd exhibited a two-phase ferrite/austenite matrix where ferrite was observed at the dendrite cores (e.g., Fig. 1a). This morphology is typical for a primary ferrite solidification mode, and this mode is consistent with that predicted from the Welding Research Council (WRC) 1992 constitution diagram[9] for the heat of 316L used in this work. Alloys with 8 and 10 wt.% Gd exhibited a single-phase matrix, which, as shown below, was fully ferritic. Interdendritic constituents can be observed in the alloys, and the amount increases with increasing Gd concentration.

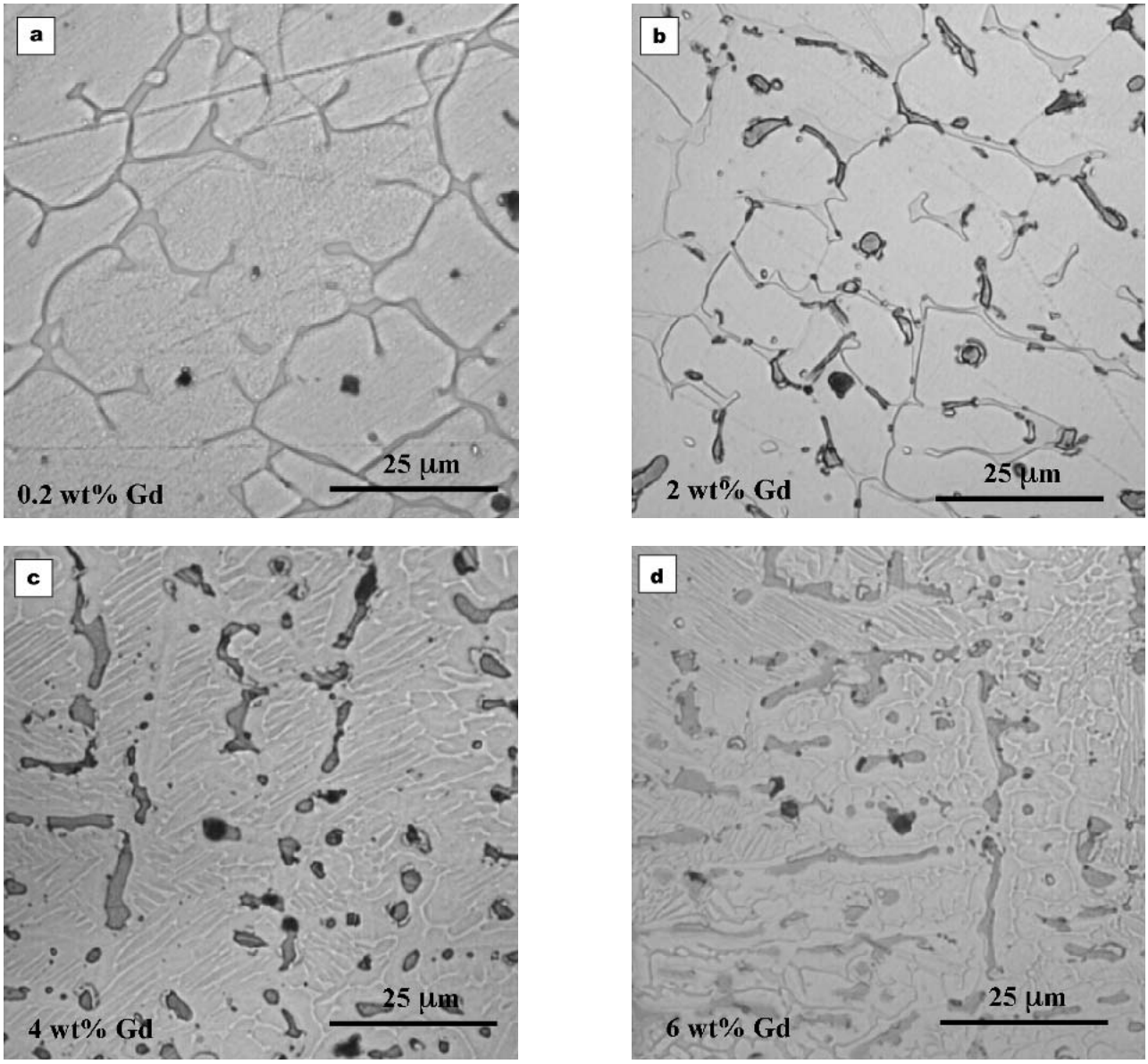


**Fig. 1** LOM photomicrographs of melt buttons with 0.2, 2, 4, and 6 wt.% Gd

**Table 3 Structure and Lattice Parameters of Relevant Binary Gd Compounds**

| Formula | Structure | Space Group | *a*, nm | *b*, nm | *c*, nm |
|---|---|---|---|---|---|
| $Gd_3Ni$ | Orthorhombic | *Pnma* | 0.695 | 0.968 | 0.636 |
| GdNi | Orthorhombic | *Cmcm* | 0.3766 | 1.0316 | 0.4244 |
| $GdNi_2$ | Cubic | $Fd\bar{3}m$ | 0.7224 | … | … |
| $GdNi_3$ | Rhombohedral | $R\bar{3}m$ | 0.499 | 0.499 | 2.454 |
| $Gd_2Ni_7$ | Rhombohedral | $R\bar{3}m$ | 0.496 | 0.496 | 3.614 |
| $Gd_2Ni_7$ | Rhombohedral | $R\bar{3}m$ | 0.496 | 0.496 | 2.409 |
| GdNi5 | Hexagonal | *P6/mmm* | 0.4902 | 0.4902 | 0.3964 |
| $Gd_2Ni1_7$ | Hexagonal | $P6_3/mmc$ | 0.8336 | 0.8336 | 0.805 |
| $GdFe_2$ | Cubic | $Fd\bar{3}m$ | 0.74 | … | … |
| $GdFe_3$ | Rhombohedral | $R\bar{3}m$ | 0.5165 | 0.5165 | 2.4707 |
| $GdFe_5$ | Hexagonal | *P6/mmm* | 0.500 | 0.500 | 0.410 |
| $Gd_2Fe_{17}$ | Hexagonal | $P6_3/mmc$ | 0.850 | 0.850 | 0.835 |
| $GdFe_{8.5}$ | Hexagonal | $P6_3/mmc$ | 0.8496 | 0.8496 | 0.8345 |
| $GdFe_9$ | Rhombohedral | $R\bar{3}m$ | 0.852 | 0.852 | 1.246 |
| GdP | Cubic | $F\bar{4}3m$ | 0.5727 | … | … |

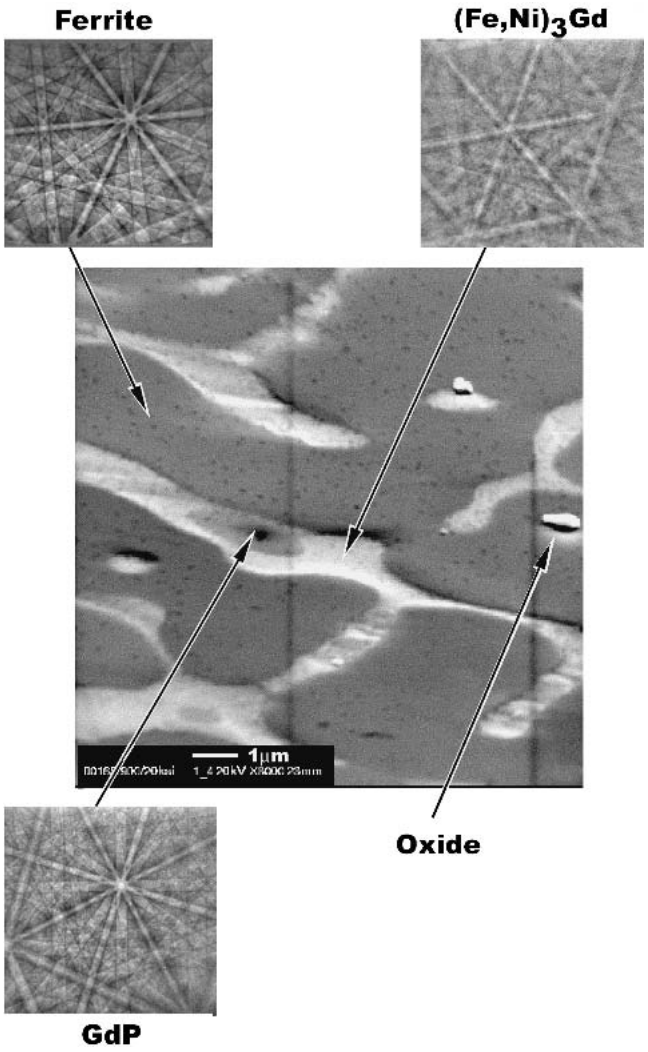


**Fig. 2** SEM photomicrograph and EBSD results obtained on 10 wt.% Gd melt button

The principal microstructural constituents identified using EBSD analysis of the button melts are summarized in Fig. 2. Table 3 shows the structure and lattice parameters of the relevant compounds in the Gd-Ni, Gd-Fe, and Gd-P binary systems. The secondary constituents shown in Fig. 2 were observed in the 10 wt.% Gd alloy, but are representative of secondary phases observed in all the other alloys, albeit in differing relative proportions. The major secondary constituent had a crystal structure consistent with the $Ni_3Gd$ gadolinide and is denoted as (Fe, Ni, Cr)$_3$Gd, since as shown later by EPMA data, Fe and small amounts of Cr apparently substitute for Ni. The matrix for the 8 and 10 wt.% Gd alloys was fully ferritic because a significant fraction of the available Ni is contained in the intermetallic phase, effectively reducing the Ni content in the matrix. As discussed later, the consumption of Ni and rejection of Cr by the intermetallic implies that the overall composition of the alloy must be adjusted in order to maintain a 316L-like composition in the alloy matrix.

As shown in Fig. 2, phosphides (GdP) were frequently observed in the button melts, and this is a consequence of the relatively high P level in the 316L base alloy. For the lower compositions of 0.1 and 0.4 wt.% Gd, most of the Gd was contained within the phosphide. A very reactive constituent, tentatively thought to be a Gd oxide, was also commonly observed and is shown in more detail in Fig. 3. This SEM micrograph shows the growth of a reaction product out of the polished surface. Although it could not be identified by the EBSD technique, EDS spectra from this constituent indicated only the presence of Gd (light elements such as O and N could not be detected with the instrument used for this analysis). It is known that Gd oxides can hydrate in the presence of water or water vapor,[10] but polishing in glycerin and transporting the prepared specimens directly to the SEM in a vacuum enclosure did not completely prevent this reaction from occurring prior to insertion of the sample into the microscope. In any case it is believed that the presence of oxygen in the button-melting environment is the source for the Gd oxides in the samples. Considering the high affinity of Gd for oxygen, this result is not surprising. A constituent containing Gd and Si, thought to be a silicide, was also occasionally observed.

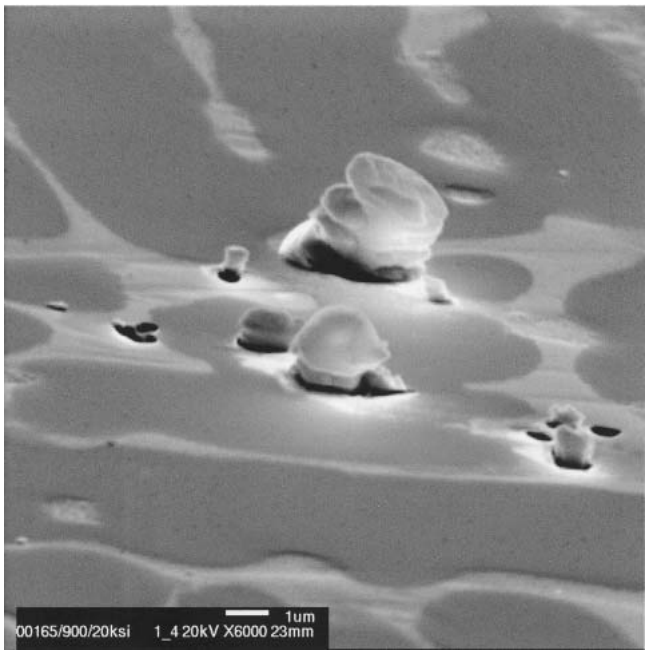


**Fig. 3** SEM micrograph showing growth of Gd oxide out of the surface of polished section

Figure 4 shows a SEM backscattered image and EPMA results that were acquired across the location denoted by the dotted line in the image. The results shown here were obtained on a 6 wt.% Gd alloy, but are representative of results obtained on other samples. (The diamond shaped impressions are hardness indentations placed on the sample to facilitate sample positioning under the electron beam.) Because of the high atomic number of Gd relative to the other alloying elements, the (Fe, Ni, Cr)$_3$Gd phase appears bright in the figure and is labeled "Gd." The regions of intermediate Gd concentrations shown in Fig. 4(b) reflect positions where the electron beam-specimen interaction volume was distributed between the austenite matrix and the (Fe, Ni, Cr)$_3$Gd phase. When the beam was

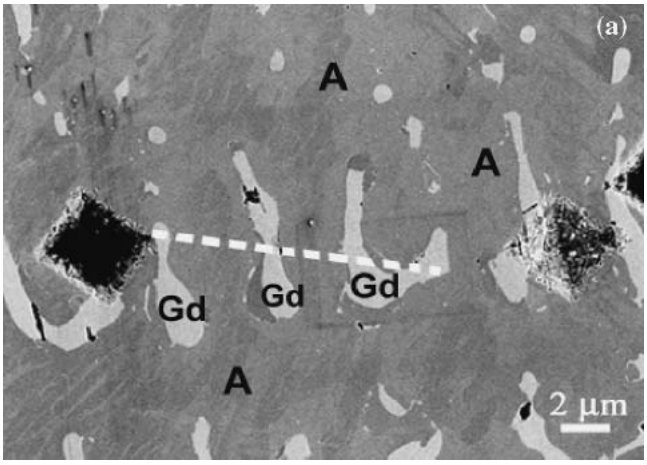


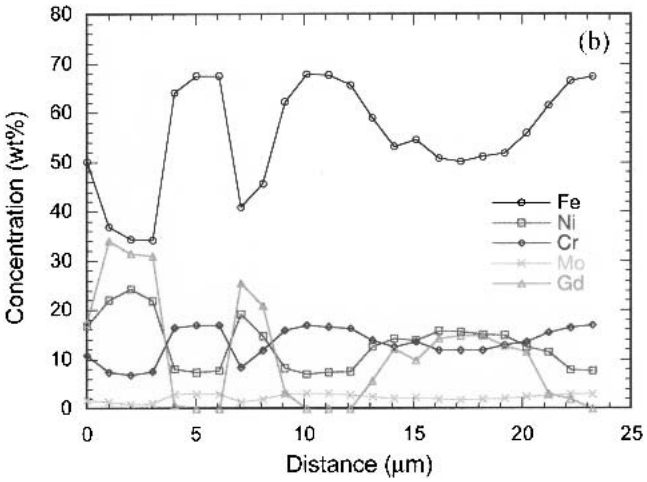


**Fig. 4** **(a)** SEM backscattered image and **(b)** typical EPMA results obtained on 6 wt.% Gd melt button

**Table 4 Composition of (Fe, Ni, Cr)$_3$Gd Phase as Determined by EPMA**

| Element | Concentration, wt.% |
|---|---|
| Fe | 21.4 |
| Ni | 28.3 |
| Cr | 3.2 |
| Mo | 0.4 |
| Mn | 0.0 |
| Si | 0.4 |
| Gd | 44.5 |

positioned entirely within the austenite matrix, no Gd was detected. Similar results were obtained when the beam was positioned on regions of ferrite in the matrix. This result indicates there is no detectable solubility of Gd in either the ferrite or austenite. Table 4 summarizes the composition of the (Fe, Ni, Cr)$_3$Gd phase. These values represent averages determined from EPMA results acquired on the (Fe, Ni, Cr)$_3$Gd phase in several alloys since no significant variation was observed from alloy to alloy. Conversion of the wt.% values shown in Table 4 to atomic fractions indicates the Gd-rich phase is (Fe, Ni, Cr)$_{0.94}$(Gd)$_{0.3}$, consistent with the (Fe, Ni, Cr)$_3$Gd stoichiometry determined using EBSD. QIA measurements, which show the vol.% of the total secondary phase as a function of Gd concentration, are presented in Fig. 5. Figure 6 shows the hardness as a function of the volume fraction of interdendritic constituent. The increased hardness suggests that the secondary constituent is relatively hard (and likely brittle) compared to the matrix, although the increasing hardness with increasing Gd concentration may also reflect the increased quantity of ferrite in the matrix at the higher Gd levels.

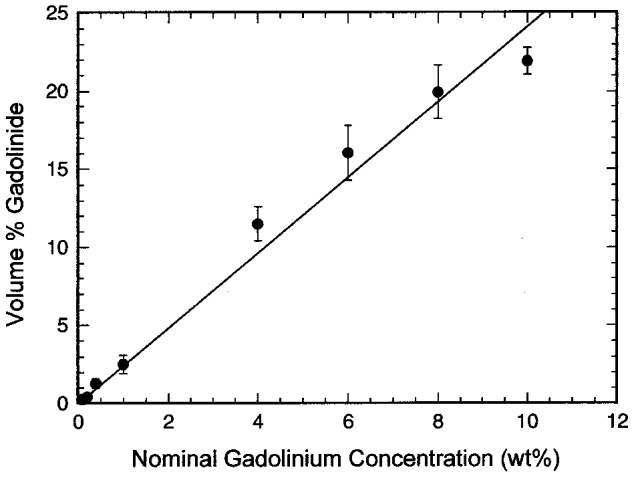


**Fig. 5** Vol.% Gd-constituent as measured by LOM

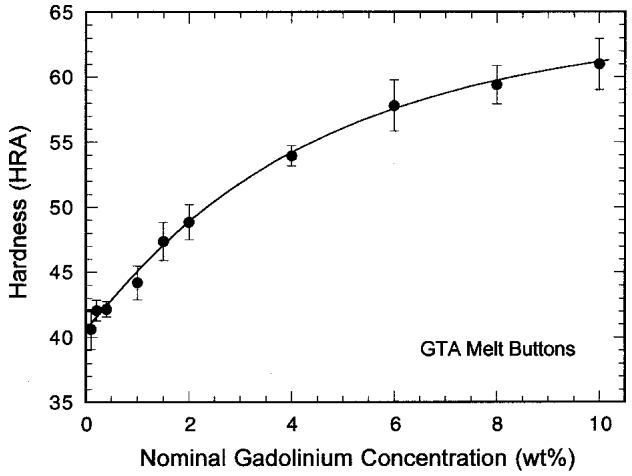


**Fig. 6** Hardness as a function of Gd concentration for the melt buttons

## 4. Discussion

The results presented above provide a general view of microstructural development in Gd-enriched 316L stainless steel. Alloys containing 0.1-6 wt.% Gd exhibit a two-phase ferrite/austenite matrix with interdendritic (Fe, Ni, Cr)$_3$Gd. As previously indicated, the 1992 WRC stainless steel constitution diagram indicates that ferrite should be the primary solidification

phase for the heat of 316L used here.[9] This is consistent with the microstructural observations, in which ferrite was observed in the dendrite cores for alloys with 0.1-6 wt.% Gd. With further cooling, most of the primary ferrite is converted to austenite by a diffusional transformation.[11,12] However, the first ferrite to form at the dendrite cores is typically enriched in Cr and depleted in Ni.[11,12] Since solid-state back diffusion is typically not fully complete, these ferrite regions remain stable and persist to room temperature. This is consistent with the microstructures observed in the alloys containing 0.1-6 wt% Gd, where the matrix consisted of austenite and ferrite, with ferrite located at the dendrite cores. However, the addition of Gd complicates the solidification process further. Since Gd is insoluble in ferrite and austenite, it will segregate preferentially to the liquid during solidification, causing a progressive enrichment of Gd in the liquid. Since the $(Fe, Ni, Cr)_3Gd$ constituent is observed in the interdendritic regions, solidification is expected to terminate by an invariant reaction, which involves the liquid and $(Fe, Ni, Cr)_3Gd$ phases. This terminal reaction will be discussed in more detail in Part II of this series of articles. Microstructural development in the 8 and 10 wt.% Gd alloys is altered by the relatively large amount of $(Fe, Ni, Cr)_3Gd$ that forms. As shown in the EPMA data (Table 4), the $(Fe, Ni, Cr)_3Gd$ phase contains approximately 28 wt.% Ni, but only approximately 3 wt.% Cr. Thus, formation of the $(Fe, Ni, Cr)_3Gd$ constituent will effectively deplete the matrix of Ni and enrich the matrix in Cr, which in turn, will stabilize the ferrite matrix, thus accounting for the fully ferritic matrix observed in the alloys with high Gd concentration.

The effects of the Gd additions can be illustrated quantitatively by mass balance considerations. Neglecting the presence of impurity constituents such as phosphides and sulfides, for any element, i, in the alloy

$$w_{i,alloy} = (w_{i,Ni_3Gd})(x_{Ni_3Gd}) + (w_{i,matrix})(x_{matrix}) \quad \text{(Eq 1)}$$

where $w_{i,y}$ denotes the wt.% of element i in constituent y (for brevity in the equations the $(Fe, Ni, Cr)_3Gd$ gadolinide is referred to as $Ni_3Gd$), and $x$ is the mass fraction of each microstructural constituent. Note that for the purposes of determining the average matrix composition, no distinction is made between the austenite and ferrite constituents within the matrix. In addition, since $x_{matrix} = 1 - x_{Ni_3Gd}$,

$$w_{i,matrix} = \frac{w_{i,alloy} - (w_{i,Ni_3Gd})(x_{Ni_3Gd})}{1 - x_{Ni_3Gd}} \quad \text{(Eq 2)}$$

Since Eq 2 requires knowledge of the mass fraction of the gadolinide and Fig. 5 only describes this quantity in terms of volume fraction, it is appropriate to use an ideal measure of mass fraction of the constituent. Rewriting Eq 1 in terms of Gd,

$$w_{Gd,alloy} = (w_{Gd,Ni_3Gd})(x_{Ni_3Gd}) + (w_{Gd,matrix})(x_{matrix}) \quad \text{(Eq 3)}$$

Since Gd was not detected in the matrix of any alloy, we can reasonably assume $w_{Gd,matrix} = 0$, and

$$x_{Ni_3,Gd} = \frac{w_{Gd,alloy}}{w_{Gd,Ni_3Gd}} \quad \text{(Eq 4)}$$

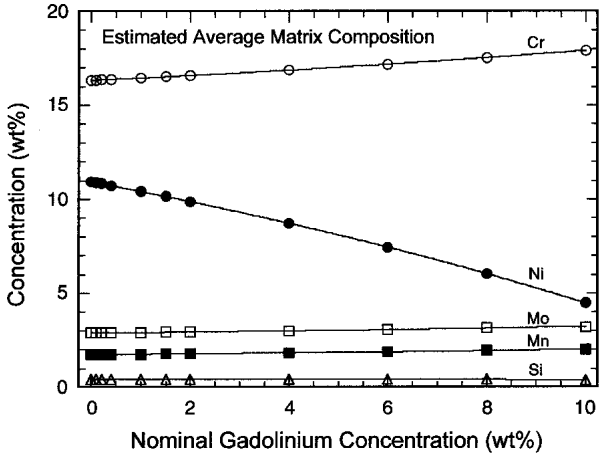


**Fig. 7** Calculated average matrix composition for the range of Gd levels examined in this work. The calculation is based on the measured composition of the Gd-containing intermetallic

Thus, the mass fraction of $Ni_3Gd$ in the alloy can be estimated by Eq 4 and the average concentration of each element in the matrix can be obtained from Eq 2 by using the gadolinide composition given in Table 4. The results of these estimates are shown in Fig. 7 and represent the expected matrix compositions for clean (low oxygen and phosphorus) alloys over the range of Gd levels examined in this study. As noted above, the direct addition of Gd to the 316L base alloy results in a depletion of Ni, and an enrichment of Cr, Mo, Mn, and Si within the matrix. For lower Gd alloys, which contain ferrite and austenite within the matrix, the compositions of Fig. 7 represent the overall average composition of these two constituents.

The results of Fig. 7 can be used to describe the effect of Gd on the resultant microstructure. This is illustrated in Fig. 8, which presents a portion of the WRC 1992 diagram[9] for predicting the solidification mode and ferrite content of stainless steels. Superimposed on the diagram are the matrix compositions from Fig. 7 for the 0-10 wt% Gd alloys. As shown, the matrix compositions move toward the lower right portion of the diagram (decreasing Ni equivalent, $Ni_{eq}$, and increasing Cr equivalent, $Cr_{eq}$) with increasing Gd content. Thus, as was observed, the matrix of the alloys can be expected to change from ferrite/austenite to fully ferritic on increasing Gd level. It should be noted that the ferrite number shown on the diagram does not simply relate to volume percentage ferrite,[13,14] so that accurate estimates of the volume fraction ferrite in the test alloys cannot be accurately inferred from this diagram. Nevertheless, the diagram implies that a fully ferritic matrix should be observed at high Gd levels. For the experimental alloys, this transition was observed to occur between 6 and 8 wt.% Gd. It should also be realized that the diagram of Fig. 8 is not a true phase diagram, and kinetic effects can alter the actual amount of ferrite present (the original WRC 1992 diagram was determined for solidification conditions and rates typical of shielded metal arc welding). Thus, the principal value of Fig. 7 is to phenomenologically illustrate the effects of Gd additions on matrix phase stability. In this sense the Gd can be viewed as a ferrite stabilizer, and this is a consequence of the fact that Gd additions effectively reduce the matrix $Ni_{eq}$ and increase the matrix $Cr_{eq}$.

**Table 5 Target Matrix Composition for the Large-Scale Heats, wt.%**

| Element | Concentration, wt.% |
|---|---|
| Fe | Balance |
| Ni | 11.50 |
| Cr | 16.75 |
| Mo | 2.85 |
| Mn | 1.75 |
| Si | 0.10 |

## 5. Implications for Alloy Design

The overall goal of this work is to produce a Gd-containing alloy with a 316L matrix composition, and the results presented above provide useful insight into preliminary alloy design strategies. The EPMA data demonstrate that Gd is essentially insoluble in austenite and ferrite. Thus, all of the Gd will exist within the $(Fe, Ni, Cr)_3Gd$ constituent. Depending on impurity levels, specifically P and O, some of the Gd may also be present in unwanted Gd phosphides and oxides. Therefore, the overall alloy composition must be adjusted as a function of Gd concentration in order to achieve the desired matrix composition, and this can be accomplished through the use of Eq 1 and 4.

In order to determine the final target compositions for the large-scale heats described in Part 2 of this research, a decision must also be made as to the desired matrix composition. For 316L type alloys, the conventional approach is to balance the Cr and Ni levels (or more specifically the $Cr_{eq}$ and $Ni_{eq}$) such that primary ferrite solidification is favored.[11,12] The underlying reason for this approach is that weldability is generally superior for alloys that solidify as primary ferrite, and then transform to austenite during cooling. In the absence of a compelling reason to base the matrix composition on other considerations, this approach was taken in the current work.

Thus, the matrix composition was defined on conventional 316L weldability considerations and is shown in Table 5. This composition has WRC Cr and Ni equivalents of 19.60 and 12.78, respectively, a $Cr_{eq}/Ni_{eq}$ ratio of 1.53, and would be expected (in the absence of the Gd-containing constituents) to solidify as primary ferrite. It should also be noted that the desired Si level is significantly lower than that for typical commercial heats. This adjustment was made to reduce the tendency for formation of gadolinium silicides, which were occasionally observed in the button melts. Since Si is principally added to stainless steels to improve high-temperature (greater than about 500 °C) oxidation resistance, it is believed that the lower Si content should not adversely affect low temperature corrosion performance.

In the Results Section, it was noted that the button melts contained a significant amount of Gd-containing oxides and phosphides, which were not related to the Gd intermetallic phases (carbides and nitrides were not observed). As discussed, the oxides are a significant problem because of their apparent reactivity with water and/or water vapor. It is believed that the oxides were primarily the result of the melting procedures used, which illustrates the need for careful control of the melting and ingot-casting environment. The P and S levels are primarily controlled by the chemistry of the raw materials rather than by the melting environment. The P level for the base 316L alloy was relatively high for a commercial heat, while the S level was low, and this accounts for the relative proportions of these constituents in the button melts. The phosphides and sulfides significantly affect the microstructure, so that control of their levels is considered important. Therefore, the P and S for the large-scale heats were specified at 0.002 wt.% maximum. Carbon and nitrogen levels were set at 0.03 wt.% maximum and are similar to conventional low carbon austenitic stainless steels.

Selection of Gd levels that are appropriate for the large-scale heats is somewhat more complex. Clearly, neutron absorption is a major requirement, and comparison[15] of the absorption characteristics of Gd and B alloyed stainless steel composition show that a 0.4 wt.% Gd alloy should have absorption characteristics similar to a 1.74 wt.% B alloy (a typical commercial borated stainless steel composition). However, it is also desirable to determine a maximum Gd level that is commensurate with acceptable mechanical properties. In an effort to determine the likely effects of the Gd additions on the mechanical properties, an assessment[15] of existing data[1,2,16] for borated stainless steels was conducted. This assessment was based on the rationale that the microstructures of the B and Gd alloyed materials are similar in character. Both alloy systems (borated stainless steel and Gd stainless steel) consist of a hard dispersed phase in a relatively soft and ductile stainless steel matrix. Thus, the borated stainless steel data can be used as a guide for selecting compositions for the large-scale trial Gd-alloy heats. Because alloy strength issues can usually be accommodated by design, the assessment[15] was focused on impact energy response, and indicated that a gadolinide volume percentages of 10% and lower should meet current impact energy requirements for nuclear applications. In order to define the Gd levels for the large-scale heats, it is therefore required to determine the volume fraction of gadolinide as a function of Gd concentration. However, given the scatter in the experimental measurements of this relationship (Fig. 5) and the prevalence of other Gd-containing constituents (e.g., oxides and phosphides) in the button melts, it was decided to determine this relationship from mass balance considerations. As shown earlier, the mass fraction gadolinide is related through Eq 4 to the bulk and gadolinide Gd concentrations. It therefore remains to convert the mass fraction estimates to volume percentages (vol.%). However, since the matrix can contain both ferrite and austenite at unknown levels [although the target matrix composition (Table 5) should have a ferrite number of 4], this conversion cannot be made directly or taken from Fig. 8. Therefore, bounding estimates were made by using densities for fully ferritic and fully austenitic matrices. For these estimates, densities for typical ferritic ($\rho = 7.7$ g/cm$^3$) and austenitic ($\rho = 7.95$ g/cm$^3$) stainless steels were used along with the density for $Ni_3Gd$ ($\rho = 9.41$ g/cm$^3$). Figure 9 shows the calculated gadolinide vol.% for the melt buttons along with the measured gadolinide vol.% taken from Fig. 5. As shown, the assumption of either ferritic or austenitic matrices makes little difference in the expected vol.% as a function of the Gd level. Moreover, irrespective of the matrix assumption, the calculated vol.% are significantly lower than the measured values. It is believed that the difference is probably due to the etching pro-

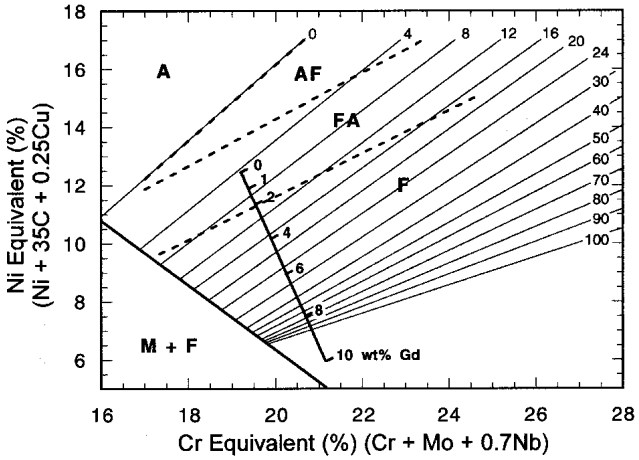


**Fig. 8** WRC 1992 Diagram showing locations of average matrix compositions for 0-10 wt.% Gd alloys

**Table 6 Target Compositions for the Large Scale Heats, wt.%**

| Gd | Fe | Ni | Cr | Mo | Mn | Si |
|---|---|---|---|---|---|---|
| 0 | 67.1 | 11.5 | 16.8 | 2.9 | 1.75 | 0.10 |
| 0.4 | 66.7 | 11.7 | 16.6 | 2.8 | 1.73 | 0.10 |
| 1.0 | 66.1 | 11.9 | 16.5 | 2.8 | 1.71 | 0.11 |
| 2.0 | 65.1 | 12.3 | 16.2 | 2.7 | 1.67 | 0.11 |
| 4.0 | 63.1 | 13.0 | 15.6 | 2.6 | 1.60 | 0.13 |
| 6.0 | 61.1 | 13.8 | 15.0 | 2.5 | 1.52 | 0.14 |

P and S both as low as achievable and <0.002 wt.%
C and N both <0.03 wt.%

cedure used to prepare the samples for LOM, which would result in an erroneously high measurement of vol.%. From Fig. 9 it is seen that a Gd level of approximately 6 wt.% corresponds to a gadolinide vol.% of 10%. Thus, the range of Gd concentrations selected for the large-scale heats was limited to 0-6 wt%. The specific concentrations selected for study were 0, 0.4, 1.0, 2.0, 4.0, and 6.0 wt.% Gd.

From the preceding considerations, the target compositions for the six large-scale heats were defined and are shown in Table 6. These compositions were determined by using a procedure that is essentially the reverse of that used to construct Fig. 7. That is, from the measured composition of the gadolinide (Table 4) and the selected bulk Gd concentrations, the expected mass fraction gadolinide was calculated by using Eq 4. The bulk concentrations for the remaining alloying elements were then calculated by inserting this quantity and the desired matrix concentration for each element into Eq 1. As a consequence of the high Ni content of the gadolinide, the overall Ni level must be increased with increasing Gd level. Conversely, the low Cr, Mo, and Mn concentrations in the intermetallic result in a lowering of the overall levels of these elements with increasing Gd content. Alloys with the compositions shown in Table 6 were fabricated by vacuum induction melting,and analytical results for these trial heats are discussed in Part 2 of this article.

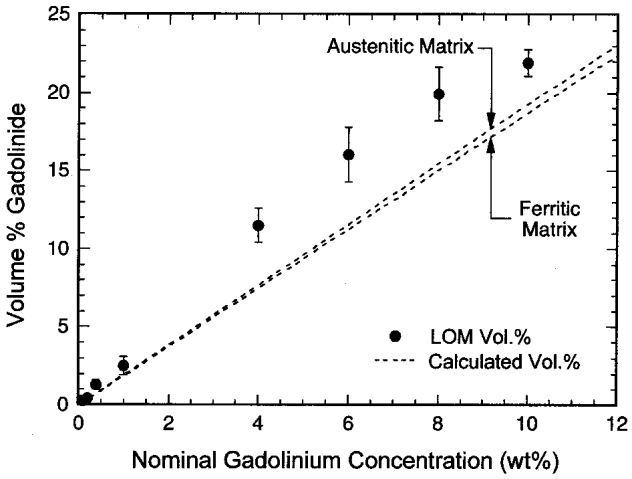


**Fig. 9** Measured and calculated vol.% of gadolinide in the Gd containing stainless steels. The lower and upper bounds for the estimate represent those obtained by assuming fully ferritic or fully austenitic matrices, respectively

## 6. Conclusions

The influence of Gd on the microstructure and hardness of 316L stainless steel was examined by various microstructural characterization techniques. The following conclusions can be drawn from this research:

- Gd exhibits no detectable solubility in the austenitic or ferritic matrix of stainless steels. Most of the Gd is contained in an (Fe, Ni, $Cr)_3Gd$ intermetallic. This phase contains approximately 28 wt.% Ni/3 wt.% Cr and, as a result, depletes the stainless steel matrix of Ni and provides enrichment of Cr.
- Depending on the levels of P, S, and O, unwanted Gd phosphides, sulfides, and oxides will also form. Thus, levels of these elements should be minimized in 316L stainless steel alloyed with Gd.
- At Gd concentrations higher than approximately 8 wt.%, sufficient quantities of the (Fe, Ni, $Cr)_3Gd$ intermetallic form that deplete the matrix in Ni and enrich the matrix in Cr to the point where austenite is no longer stable, and the matrix becomes fully ferritic.
- The hardness of Gd stainless steel increases with increasing volume fraction of the (Fe, Ni, $Cr)_3Gd$ intermetallic. This increase is likely due to both the hardening effect of the gadolinide constituent and well as the increasing ferrite content in the matrix.
- A simple mass balance procedure can be used for determining the nominal alloy composition required to produce 316L type matrix compositions at any Gd level.

### Acknowledgements

Thanks are due to D. Branagan of INEEL for producing the arc melts and Aaron Hall of Sandia for his thoughtful review of the manuscript. This work was supported by the U.S. Department of Energy, Assistant Secretary for Environmental Man-

agement, under D.O.E. Idaho Operations Office Contract No. DE-AC07-99ID13727. This work was performed at Lehigh University, Sandia National Laboratories, and Idaho National Engineering and Environmental Laboratory through support from the National Spent Nuclear Fuel Program. Sandia is a multiprogram laboratory operated by Sandia Corporation, a Lockheed Martin Company, for the U.S. Department of Energy under Contract DE-AC04-94AL8500.

## References

1. C.V. Robino and M.J. Cieslak: "Fusion Welding of a Modern Borated Stainless Steel," *Welding J. Res. Suppl.*, 1997, *76,* pp. 11s-23s.
2. C.V. Robino and M.J. Cieslak: "High-Temperature Metallurgy of Advanced Borated Stainless Steels," *Metall. Mater. Trans. A*, 1995, *26A,* pp. 1673-85.
3. R.A. Van Konynenburg, P.G. Curtis, and T.S.E. Summers: "Scoping Corrosion Tests on Candidate Waste Package Basket Materials for the Yucca Mountain Project," Report UCRL ID 130386, Lawrence Livermore National Laboratory, Livermore, CA, 1998.
4. L. Hull, M. Pace, P. Lessing, R. Rogers, R. Mizia, A. Propp, E. Shaber, and L. Taylor: "Advanced Neutron Absorbers for DOE SNF Standardized Canisters—Feasibility Study," Idaho National Engineering and Environmental Laboratory Report DOE/SNF/REP-057 Rev. 0, Idaho Falls, ID, 2000.
5. Z. Jianxuan and Z. Huaiying: "The Phase Diagram of Fe-Gd-Ni Ternary System," *Zhongguo Xitu Xuebao* (*J. Chin. Rare Earth Soc.*), 1986, *4*(2), pp. 79-81 (in Chinese).
6. H. Baker, ed.: *Alloy Phase Diagrams, ASM Handbook,* Vol. 3, ASM International, Materials Park, OH, 1992, pp. 2-194 and 2-220.
7. *The Handbook of Binary Phase Diagrams,* W.G. Moffat, ed., General Electric Company, Schenectady, New York, 1983.
8. J.I. Goldstein, D.E. Newbury, P. Ecglin, D.C. Joy, C. Fiori, and E. Lifshin: *Scanning Electron Microscopy and X-Ray Microanalysis*, Plenum Press, New York, 1981, p. 305.
9. D.J. Kotecki and T.A. Siewert: "WRC-1992 Constitution Diagram for Stainless Steel Weld Metals: A Modification of the WRC-1988 Diagram," *Welding J. Res. Suppl.*, 1992, *71*(5), pp. 171s-178s.
10. R.C. Weast, ed.: *Handbook of Chemistry and Physics*, CRC Press, Cleveland, Ohio, 1975, p. B-95.
11. J.A. Brooks and A.W. Thompson: "Microstructural Development and Solidification Cracking Susceptibility of Austenitic Stainless Steel Welds," *Int. Metals Rev.,* 1991, 36, pp. 16-44.
12. J.A. Brooks and J.C. Lippold: "Selection of Wrought Austenitic Stainless Steels" in *ASM Metals Handbook,* Vol. 6, ASM International, Metals Park, OH, 1993, pp. 456-470.
13. D.J. Kotecki: "Extension of the WRC Ferrite Number System," *Welding J. Res. Suppl.,* 1982, *61,* pp. 352s-361s.
14. D.J. Kotecki: "Ferrite Determination in Stainless Steel–Advances since 1974," *Welding J. Res. Suppl.*, 1997, *76,* pp. 24s-37s.
15. J.N. DuPont, Z.Q. Liu, S.W. Banovic, D.B. Williams, C.V. Robino, J.J. Stephens, P.M. McConnell, R.E. Mizia, E.L. Shaber, and D.J. Branagan: "Development of Gadolinium-Containing Stainless Steels," Idaho National Engineering and Environmental Laboratory Report, DOE/SNF/REP-066, Idaho Falls, ID, Jan 2001.
16. J.J. Stephens, K.B. Sorenson, and P. McConnell: "Elevated Temperature Tensile Properties of Borated 304 Stainless Steel: Effect of Boride Dispersion on Strength and Ductility" in *Proceedings PATRAM 92,* Yokohama, Japan, Aug 1992.